# Three-Dimensional Vibrational Imaging by Coherent Anti-Stokes Raman Scattering

Andreas Zumbusch,* Gary R. Holtom, and X. Sunney Xie†

*Pacific Northwest National Laboratory, William R. Wiley Environmental Molecular Sciences Laboratory, P.O. Box 999, K8-88, Richland, Washington 99352*

(Received 9 December 1998)

A multiphoton microscopy based on coherent anti-Stokes Raman scattering is accomplished with near-infrared ultrashort laser pulses. We demonstrate vibrational imaging of chemical and biological samples with high sensitivity, high spatial resolution, noninvasiveness, and three-dimensional sectioning capability. [S0031-9007(99)09110-3]

PACS numbers: 87.64.Je, 87.15.Mi, 87.16.Tb, 87.64.Vv

Confocal [1] and multiphoton [2] fluorescence microscopy have become powerful techniques for three-dimensional imaging of chemical and biological samples, especially for live cells. This coincides with developments of various natural and artificial fluorescent probes for cellular constituents [3]. For chemical species or cellular components that either do not fluoresce or cannot tolerate labeling, infrared microscopy and spontaneous Raman microscopy can be used as contrast mechanisms based on vibrational properties. Conventional infrared microscopy is limited to low spatial resolution because of the long wavelength of light used. High resolution Raman microscopy of biological samples has been demonstrated with a confocal microscope [4]. However, the intrinsically weak Raman signal necessitates high laser powers (typically $>10$ mW) and is often overwhelmed by the fluorescence background of the sample. A multiphoton microscopy based on coherent anti-Stokes Raman scattering (CARS) [5] was put forward as an alternative way of providing vibrational contrast [6]. However, the sensitivity of CARS microscopy was limited by the nonresonant background signal, and high resolution three-dimensional sectioning was not achieved. In the study reported here, we demonstrate CARS microscopy in the chemically interesting vibrational spectral region around 3000 $cm^{-1}$ with high spatial resolution and three-dimensional sectioning capability. Most importantly, the use of near-infrared laser pulses generated by a Ti:sapphire laser ($\sim$855 nm) and an optical parametric oscillator/amplifier ($\sim$1.2 $\mu$m) allows a significant improvement in signal to background ratio in CARS detection. Unlike spontaneous Raman microscopy, the highly sensitive CARS microscopy requires only a moderate average power for excitation ($\sim$0.1 mW), tolerable by most biological samples.

CARS spectroscopy has been extensively used as a spectroscopic tool for chemical analyses in the condensed and gas phases [7]. In doing CARS spectroscopy, a pump laser and a Stokes laser beam, with center frequencies of $\nu_p$ and $\nu_S$, respectively, are spatially overlapped. The CARS signal at $2\nu_p - \nu_S$ is generated in a direction determined by the phase-matching conditions. When the frequency difference $\nu_p - \nu_S$ coincides with the frequency of a molecular vibration of the sample, the CARS signal is often strongly enhanced. As CARS is a four-wave-mixing process, the signal intensity depends nonlinearly on the incident intensities: $I_{\mathrm{CARS}} \sim I_P^2 I_S$. The energy and phase-matching diagrams are shown in Fig. 1(a). Similar to other nonlinear optical processes, high peak powers are necessary for the efficient generation of a CARS signal. These are readily available using femtosecond or picosecond light pulses, the choice of which is determined by the spectral resolution required.

For CARS microscopy, we use a lens with a high numerical aperture to focus the beams tightly. With the tight foci, the phase-matching conditions are relaxed because of the large cone of wave vectors and the short interaction length. The nonlinear intensity dependence

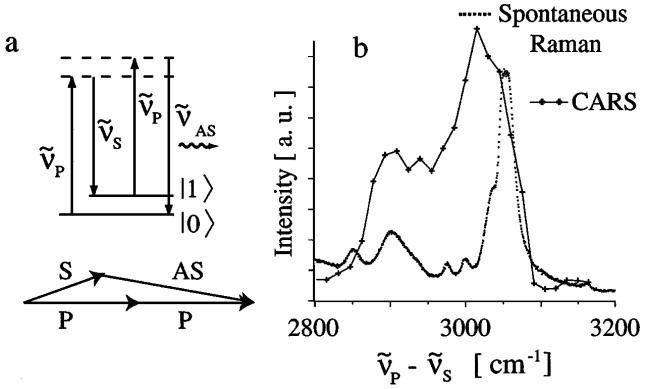


FIG. 1. (a) Energy (upper panel) and phase-matching (lower panel) diagrams for CARS. The CARS signal is due to interactions of molecules with a pump and a Stokes laser with frequencies of $\nu_p$ and $\nu_S$, respectively. When the frequency difference $\nu_p - \nu_S$ coincides with the frequency difference between the molecular vibrational levels $|0\rangle$ and $|1\rangle$, a strong CARS signal is generated. The phase-matching condition determines the direction of the anti-Stokes ($\nu_{\mathrm{AS}} = 2\nu_p - \nu_S$) beam. (b) CARS spectrum (crosses with solid line) of a 910 nm diameter polystyrene bead. The spectrum was taken at fixed $\nu_p$ while varying $\nu_S$. The CARS signal intensity at different Raman shifts $\nu_p - \nu_S$ are normalized to the background signal at the same wavelengths. The spontaneous Raman spectrum (dotted line) shows peaks for aliphatic CH (2851 and 2902 $cm^{-1}$) and aromatic CH (3054 $cm^{-1}$) vibrations, which can also be distinguished in the CARS spectrum.

 0031-9007/99/82(20)/4142(4)$15.00 

restricts the excitation to a small volume at the laser foci, similar to multiphoton fluorescence microscopy. This leads to efficient background signal rejection, reduces photodamage to the sample, and opens the possibility of three-dimensional microscopy by sectioning at different focal planes. A slight improvement in lateral resolution compared to conventional microscopy is also observed, similar to two-photon microscopy [8].

A major difference between CARS and spontaneous Raman microscopy is that CARS is a coherent process, in which the molecular vibrations in the excitation volume oscillate in phase, interfering constructively. Therefore, the CARS signal is proportional to the square of the concentration of the vibrational modes. In contrast, a spontaneous Raman or fluorescence signal is incoherent and has linear concentration dependence.

Imaging with third harmonic generation, another coherent four-wave-mixing process, has been demonstrated recently [9]. CARS microscopy is similar to this technique in that the signal is dependent on the third-order polarizability $\chi^{(3)}$, but differs in that it probes the vibrational spectral properties of $\chi^{(3)}$. In CARS microscopy, the electronic contributions to $\chi^{(3)}$ are exhibited as a nonresonant background signal with no vibrational contrast and need to be minimized. The magnitude of the nonresonant background signal is dependent on the wavelengths of the excitation lasers. In the previous CARS microscopy work using visible lasers, the CARS signal was dominated by the nonresonant background signal [6].

We use near-IR excitation pulses that do not give rise to direct electronic excitations in the sample and therefore avoid photochemical damage due to photobleaching. The use of near-IR excitation light allows two significant improvements over the previous work [6]. First, because the excitation frequency is further removed from the electronic transition, the nonresonant background signal is significantly reduced. Our CARS signal is pertinent to vibrational properties. Second, the long excitation wavelengths also minimize Rayleigh scattering in heterogeneous samples and consequently enable large penetration depths for thick samples that are desirable for many applications.

Two synchronized femtosecond pulse trains at a high repetition rate (250 kHz) are generated from a Ti:sapphire regenerative amplifier (Coherent Rega) operating at a center wavelength of 855 nm and a homebuilt optical parametric oscillator and optical parametric amplifier operating at 1.1–1.2 $\mu$m [10]. Our laser system restricts us to the frequency range of 2600–3300 $cm^{-1}$ for the Raman shifts, a region typical for C-H and N-H vibrations. However, extension to other spectral regions, such as the fingerprint region at 1000–2000 $cm^{-1}$, does not pose any notable problems. The two pulse trains with parallel polarizations are independently adjusted for bandwidths (nearly square band of 50 $cm^{-1}$ width), temporally overlapped by an optical delay line, collinearly coupled into an optical microscope, and focused on the same spot of the sample with an oil-immersion objective (Nikon Plan Apo, 60×, Na 1.4). The sample is raster scanned with a computerized $x, y$ stage (Physik Instrumente E-500), $z$ positioning being done with an independent piezoelectric element. Images are composed of 512 by 512 pixels, and a typical pixel acquisition time is 10 ms. The CARS signal is collected in the forward direction with another oil-immersion objective lens, filtered for the emission at 665–700 nm and detected with photon counting.

Figure 1(b) shows the CARS spectrum of a single carboxylated polystyrene bead of 910 nm diameter on a glass coverslip, centered to the foci. To record the spectrum, the pump wavelength was held constant at 854 nm, while the Stokes wavelength was tuned in 2 nm steps from 1.12 to 1.17 $\mu$m, corresponding to Raman shifts from 2781–3163 $cm^{-1}$. A nonresonant CARS background was present, but significantly weaker than ($<5\%$) the resonant CARS signal. Both signals have the same intensity dependence. The resonant CARS signal was normalized with the nonresonant background signal in order to compensate for intensity variations associated with the wavelength changes of the Stokes beam. The spectral resolution, given by the convolution of the spectral widths of the two exciting laser beams, lay around 60 $cm^{-1}$. Using longer laser pulses with a narrower spectrum would allow distinguishing sharper spectral features. For comparison, the spontaneous Raman spectrum of the same beads is also shown in Fig. 1(b). The peaks at 2851 and 2902 $cm^{-1}$ are assigned to aliphatic C-H stretching vibrations, while the band at 3054 $cm^{-1}$ is due to an aromatic C-H stretching vibration [11]. The peaks for the aliphatic and aromatic C-H vibrations are present in our CARS spectrum, which proves the ability of CARS microscopy to differentiate between those spectral features in polystyrene. The dip in the CARS spectrum at 3110 $cm^{-1}$ is reproducible and is caused by destructive interference of the resonant CARS signal with the nonresonant background [5].

A further proof of our detection of CARS signals is the intensity dependence. As shown in Fig. 2, the CARS signal at 3038 $cm^{-1}$, close to the center of the aromatic CH peak of polystyrene, is quadratic in $I_P$ and linear in $I_S$, as expected. Within the power range studied, no saturation is observed, which is consistent with the instantaneous nature of the scattering process. In contrast, saturation in fluorescence imaging can occur even at moderate power levels due to the relatively long fluorescence and/or triplet lifetimes. In practice, however, the laser powers usable in CARS microscopy are limited by thermal effects or by continuum generation.

The ability to generate three-dimensional CARS images is highlighted in Fig. 3, where we show images of a 4.3 $\mu$m diameter polystyrene bead surrounded by 910 nm diameter polystyrene beads, recorded at five successive heights from the surface of the glass coverslip with 1.2 $\mu$m increments. The movement of the smaller beads in and out of the image plane and the increasing diameter of the large bead in the image plane are

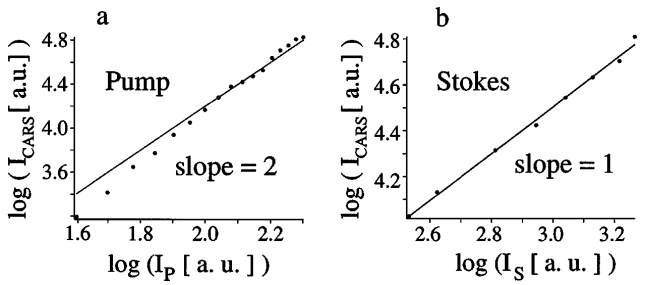


FIG. 2. Dependence of the CARS signal on the excitation powers of the pump and Stokes beams. CARS signal intensities of a polystyrene bead were measured at different excitation powers, with the laser frequencies tuned to the Raman shift of 3038 $cm^{-1}$, the aromatic C-H vibration band. (a) CARS signal as a function of the power of the pump beam ($I_P$) at 855 nm at a constant Stokes beam power ($I_S = 200$ $\mu$W) at 1.155 $\mu$m. (b) CARS signal as a function of the power of the Stokes beam at 1.155 $\mu$m and a constant Stokes beam average power ($I_P = 50$ $\mu$W) at 855 nm. Both results are consistent with $I_{\mathrm{CARS}} \sim I_P^2 I_S$.

clearly seen. Fitting the signal intensity values at different sample heights with a Gaussian function, we can infer a point-spread function with a full width at half maximum (FWHM) of 1.61 $\mu$m along the $z$ axis [12]. As noncompensated chromatical aberration is expected with the microscope objective used for both of the exciting laser wavelengths, further improvements on the $z$ resolution is expected for appropriately corrected microscope lenses and better beam qualities.

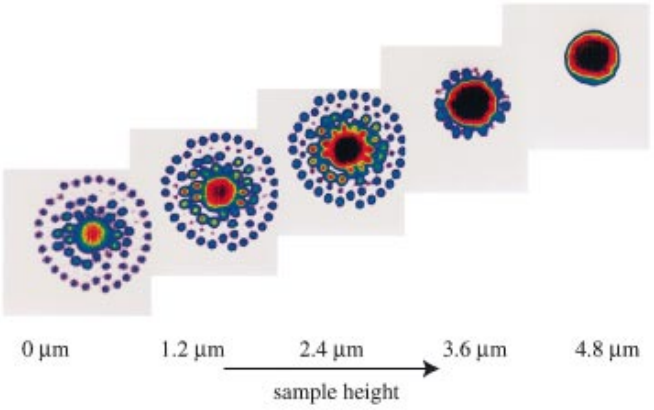


FIG. 3(color). $z$ sectioning capability of CARS microscopy. The sample consists of many polystyrene beads with 910 nm diameter surrounding a bead of the same material with 4.3 $\mu$m diameter. The beads were spin coated on a coverslip, index matched with a fluorinated oil and covered with another coverslip. A sequence of images (20 $\mu$m $\times$ 20 $\mu$m) was taken at different sample heights with an increment of 1.2 $\mu$m. The average powers incident on the sample were 120 $\mu$W at 855 nm and 50 $\mu$W at 1.155 $\mu$m. The Raman shift is 3038 $cm^{-1}$, close the maximum of the aromatic CH peak. The movement of the smaller beads into and out of the focal plane and the increase in apparent diameter of the larger bead with increasing sample height is clearly visible. From these data we can deduce a point spread function with a FWHM of 1.61 $\mu$m in the axial direction.

In an attempt to determine the sensitivity and lateral resolution, we decreased the size of the beads. Polystyrene beads of 110 nm diameter can easily be imaged. As shown in Fig. 4, the cross section of a 110 nm bead allows us to determine the lateral point spread function with FWHM of 302 nm, which is better than $\lambda/2$ for the excitation wavelengths. The bead contains $3.2 \times 10^6$ aromatic rings, which gives us an upper limit for CARS detection sensitivity under the moderate power levels used and experimental conditions to be perfected. The limiting factor in sensitivity is the nonresonant background signal from the substrate and surrounding medium.

The ability to record CARS images of live cells is demonstrated in Fig. 5. *Shewanella putrefaciens* strain CN-32 is a Gram negative bacterium [13]. Figure 5(a) shows the CARS image of individual bacteria when we tuned the laser frequencies to a Raman shift to 2878 $cm^{-1}$, the frequency of aliphatic C-H stretching vibrations. Aliphatic C-H was expected to be abundant in the lipid bilayer of the cell membrane. The bacteria were grown on a glass coverslip, immersed in $D_2O$, and covered with another coverslip. $D_2O$ was used to avoid sample heating as $H_2O$ has weak overtone absorption with an onset at around 1.15 $\mu$m [14]. The heating problem, if any, could easily be overcome by slightly shifting the wavelengths of both laser beams. For other systems, however, we found that $H_2O$ can be used as a solvent without any observable heating effects. When tuning the Raman shift away from the aliphatic C-H stretching frequencies, all image contrast was lost. Detailed features within the small bacterial cells in Fig. 5(a) could not be resolved due to the insufficient lateral resolution, comparable to two-photon microscopy (the cell width was

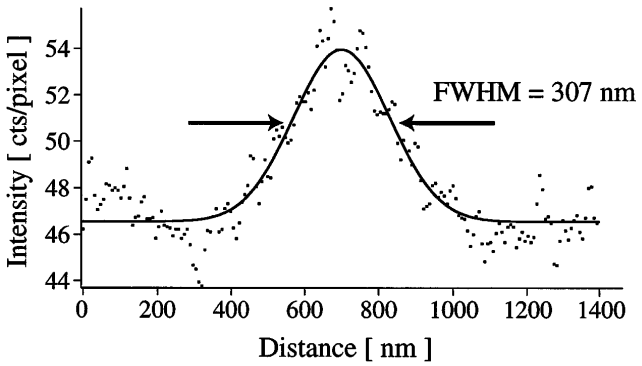


FIG. 4. Intensity profile (dotted line) from the CARS image of a 110 nm diameter polystyrene bead. The fitted Gaussian function (solid line) has a FWHM of $\Delta_1 = 307$ nm. This and a model Gaussian function with a FWHM of $\Delta_2 = 57$ nm for the square of scatter density in the probe volume allow us to calculate a point spread function with a FWHM$\Delta = \sqrt{\Delta_1^2 - \Delta_2^2} = 302$ nm for the lateral resolution. The Raman shift was tuned to 3053 $cm^{-1}$, the aromatic CH stretching vibration. The average powers incident on the sample were 100 $\mu$W at 855 nm and 50 $\mu$W at 1.157 $\mu$m. There were $3.2 \times 10^6$ aromatic rings in the bead. The collection time for each pixel was 13 ms.

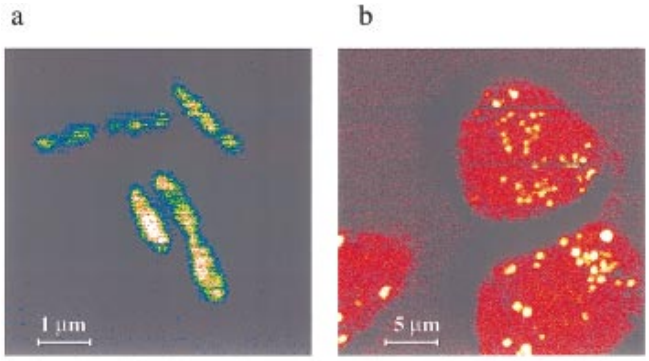


FIG. 5(color). CARS images of live cells. (a) CARS image of six live, unstained bacteria of the type *Shewanella putrefaciens*, strain CN-32, in $D_2O$. Average powers incident at the sample were 100 $\mu$W at 855 nm and 100 $\mu$W at 1.134 $\mu$m. The Raman shift is 2878 $cm^{-1}$, in the spectral region of aliphatic CH vibrations. (b) CARS image of three live, unstained HeLa cells in aqueous HEPES buffer solution. Average powers incident at the sample were 50 $\mu$W at 853 nm and 50 $\mu$W at 1.135 $\mu$m. The Raman shift is 2913 $cm^{-1}$, in the spectral region of aliphatic CH vibrations. The bright features are mitochondria that are rich in aliphatic CH. Both images are 512 by 512 pixels with collection times of 10 ms per pixel.

smaller than 500 nm). However, the CARS image shows the high sensitivity, enabling the imaging of unstained live bacterial cells.

CARS microscopy can resolve cellular components within eucaryotic cells. Figure 5(b) shows an image of live HeLa cells in an aqueous HEPES (N-[2-Hydroxyethyl] piperazine-N′-[2-ethanesulfonic acid]) buffer solution, again with the Raman shift tuned to the aliphatic C-H stretching region. The bright features of a size of approximately 1 $\mu$m within the cells are attributed to mitochondria that are rich in aliphatic C-H. This assignment was confirmed by specific fluorescence labeling of mitochondria with Rhodamine 123 (Molecular Probes). Tuning the Raman shift away from the frequency of aliphatic C-H stretching vibrations led to a complete loss of CARS contrast. The average power levels used for recording the image shown in Fig. 5(b) were 50 $\mu$W at 853 nm and 50 $\mu$W at 1.135 $\mu$m. No photodamage of the living cells was observed during the image acquisition of 43 min. The length of acquisition time was limited only by the photon counting scheme in which the count rate was kept below 10% of the laser repetition rate to avoid saturation. Analog detection is expected to allow faster acquisition.

CARS microscopy does not rely on the presence of fluorophores, but retains the resolution and three-dimensional sectioning capability of confocal and multiphoton fluorescence microscopy. Complementary to these techniques, CARS microscopy provides a contrast mechanism based on vibrational spectroscopy. The vibrational contrast mechanism, combined with an unprecedented high sensitivity at a biologically tolerable laser power level, provides exciting possibilities for microscopic investigations of chemical and biological samples, especially live cells.

We thank Matt Gray and Noelle Metting for the preparation of biological samples and Erik Sánchez for the programming of the data acquisition software. This work was supported by the U.S. Department of Energy's (DOE) Office of Basic Energy Sciences, with instrument development support from DOE's Office of Biological and Environmental Research for the construction of the Environmental Molecular Science Laboratory. PNNL is operated by Battelle for the DOE. A. Z. gratefully acknowledges support from the Alexander von Humboldt Foundation.

*Present address: Institute für Physikalische Chemie, Universität München, Butenandtstr. 5-13 Haus E, D-81377 München, Germany.

†Present address: Harvard University, Department of Chemistry and Chemical Biology, 12 Oxford Street, Cambridge, MA 01238.

[1] See articles in *Handbook of Biological Confocal Microscopy*, edited by J. B. Pawley (Plenum, New York, 1995).

[2] W. Denk, J. H. Strickley, and W. W. Webb, Science **248**, 73 (1990).

[3] For a review see R. Y. Tsien and A. Miyawaki, Science **280**, 1954 (1998).

[4] G. J. Puppels *et al.*, Nature (London) **347**, 301 (1990); N. M. Sijtsema *et al.*, Appl. Spectrosc. **52**, 348 (1998).

[5] Y. R. Shen, *The Principles of Nonlinear Optics* (John Wiley and Sons Inc., New York, 1984), p. 267.

[6] M. D. Duncan, J. Reintjes, and T. J. Manuccia, Opt. Lett. **7**, 350 (1982); Opt. Eng. **24**, 352 (1985).

[7] For reviews see N. Bloembergen, Pure Appl. Chem. **10**, 1229 (1987); S. Maeda, T. Kamisuki, and Y. Adachi, in *Advances in Non-linear Spectroscopy*, edited by R. J. H. Clark and R. E. Hester (John Wiley and Sons Ltd., New York, 1988), p. 253; J. Nibler, *ibid.*, p. 1.

[8] C. J. R. Sheppard and M. Gu, Optik **86**, 104 (1990).

[9] Y. Barad, H. Eisenberg, M. Horowitz, and Y. Silberberg, Appl. Phys. Lett. **70**, 922 (1997); M. Müler, J. Squier, K. R. Wilson, and G. J. Brakenhoff, J. Microsc. **191**, 266 (1998).

[10] G. Holtom, R. Crowell, and X. S. Xie, J. Opt. Soc. Am. B **12**, 1723 (1995).

[11] B. Schrader, in *Infared and Raman Spectroscopy*, edited by B. Schrader (VCH, Weinheim, 1995), p. 187.

[12] The Gaussian function fitted to the signal intensity as a function of sample height has a FWHM of $\Delta_1 = 1.69$ $\mu$m. A model Gaussian function with a FWHM of $\Delta_2 = 485$ nm is used as an expression of the square of scatter density in the probe volume for a 910 nm bead. We deduce a point spread function with a FWHM $\Delta = \sqrt{\Delta_1^2 - \Delta_2^2} = 1.61$ $\mu$m for the resolution in the $z$ direction.

[13] J. K. Fredrickson, J. M. Zachara, D. W. Kennedy, H. Dong, T. C. Onstott, N. W. Hinman, and S. W. Li, Geochim. Cosmochim. Acta **62**, 3239 (1998).

[14] I. R. Levin and E. N. Lewis, Anal. Chem. **62**, 1101A (1990).